Chinese Physics Letters **42**, 110703 (2025) **Express Letter**

Physical Origin of Current-Induced Switching Angle Shift in Magnetic Heterostructures

Xiaomiao Yin[1,3,4†], Guanglei Han[1,2†], Guowen Gong[1,2†], Jun Kang[3,4], Changmin Xiong[4,5], and Lijun Zhu[1,2*]

[1]*State Key Laboratory of Semiconductor Physics and Chip Technologies, Institute of Semiconductors, Chinese Academy of Sciences, Beijing 100083, China*
[2]*Center of Materials Science and Optoelectronics Engineering, University of Chinese Academy of Sciences, Beijing 100049, China*
[3]*Beijing Computational Science Research Center, Beijing 100193, China*
[4]*Department of Physics, Beijing Normal University, Beijing 100875, China*
[5]*Key Laboratory of Multiscale Spin Physics, Ministry of Education, Beijing Normal University, Beijing 100875, China*

(Received 25 August 2025; accepted manuscript online 10 September 2025)

Accurate quantification of the spin–orbit torques (SOTs) is critical for the identification and applications of new spin-orbitronic effects. One of the most popular techniques to quantify the SOTs is the "switching angle shift", where the applied direct current is assumed to shift, via domain wall depinning during anti-domain expansion, the switching angle of a perpendicular magnetization in a linear proportional manner under a large rotating magnetic field. Here, we report that, for the most commonly employed perpendicular magnetization heterostructures in spintronics (e.g., those based on FeCoB, Co, and Co/Ni multilayers), the switching angle shift considerably misestimates the SOT within the domain wall depinning analysis of the slope of linear-in-current scaling and may also have a non-zero residual value at zero direct current. Our experiments and simulations unveil that the switching angle shift is most likely dominated by chiral asymmetric nucleation rather than expansion of anti-domains. The in-plane field from external magnets and current-induced SOTs lowers the perpendicular nucleation field and thus reduces the required switching angle, ultimately leading to an underestimation of SOTs by domain wall depinning analysis. These results have advanced our understanding of magnetization switching in spintronic devices.

DOI: 10.1088/0256-307X/42/11/110703 CSTR: 32039.14.0256-307X.42.11.110703

Current-induced spin–orbit torques (SOTs) have attracted blooming interest in the field of spintronics for their great potential in switching magnetization for fast, low-power memory and logic technologies.[1–4] Accurate quantification of the SOT efficiency ($\xi^j_{\rm DL}$) is critical not only for the usefulness evaluation of new magnetic heterostructures but also for exploring the in-depth mechanisms of SOTs[5–12] and magnetization switching.[14,15] One of the most popular SOT analyses for magnetic heterostructures with perpendicular magnetic anisotropy (PMA) is the current-induced "switching angle shift",[15–27] which collects the Hall resistance ($R_{\rm H}$) as a function of the elevation angle (β, close to 0° or 180°) of a large magnetic field (H_{xz}) relative to the applied direct current (I, in x direction), that generates a damping-like SOT field ($H_{\rm DL}$) via the spin Hall effect [Figs. 1(a)–1(c)]. Assuming a switching mechanism based on conventional chiral domain wall depinning,[28–32] the switching angle shift analysis predicts

$$H_{\rm DL} \approx H_{xz}\Delta\beta, \tag{1}$$

where the switching angle shift is defined as $\Delta\beta \equiv (\beta_\downarrow + \beta_\uparrow)/2$ for $\beta \to 0°$ and $180° - (\beta_\downarrow + \beta_\uparrow)/2$ for $\beta \to 180°$, with $\beta_\downarrow$ and $\beta_\uparrow$ being the switching angles for the down-up and up-down switching. Thus, the switching angle shift model expects $\Delta\beta$ to scale inversely with H_{xz} for a given current density (j) in the spin current-generating layer, inearly with j for a given H_{xz}, and to be exactly zero at zero current density ($j = 0$). With the $\Delta\beta/j$ ratio, $\xi^j_{\rm DL}$ can be estimated as[28–32]

$$\xi^j_{\rm DL} = (4e/\pi\hbar)\mu_0 M_{\rm s} t_{\rm FM} H_{xz}\Delta\beta/j \tag{2}$$

for the domain wall depinning switching. Here, e is the elementary charge, $\hbar$ the reduced Planck's constant, μ_0 the permeability of vacuum, $t_{\rm FM}$ the layer thickness of the magnetization, $M_{\rm s}$ the saturation magnetization.

Since 2012, current-induced switching angle shift has been widely employed and closely related to the evolution of the spintronics frontiers by evaluating the efficiencies and anisotropies of the SOTs of transverse spins, out-of-plane SOT fields, and the Dresselhaus and Rashba effective fields in a variety of magnetic heterostructures, ranging from heavy metal/ferromagnet bilayers,[21] single-layer ferromagnetic semiconductors (e.g., GaMnAs),[23]

†These authors contributed equally to this work.
*Corresponding author. Email: ljzhu@semi.ac.cn
© 2025 Chinese Physical Society and IOP Publishing Ltd. All rights, including for text and data mining, AI training, and similar technologies, are reserved.

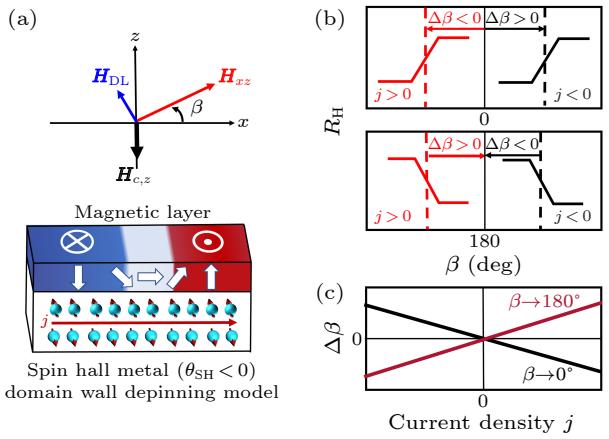

Fig. 1. Principle of the switching angle shift analysis. (a) Effective magnetic fields during SOT switching via domain wall depinning in spin Hall metal/ferromagnet bilayer (for the case of a negative spin Hall ratio θ_{SH}). (b) Hall resistance vs. the elevation angle (β) of the applied magnetic field near 0° and 180°, indicating the sign of the switching angle shift ($\Delta\beta$). (c) Expected dependence of $\Delta\beta$ on direct current density for $\beta \to 0°$ and for $\beta \to 180°$.

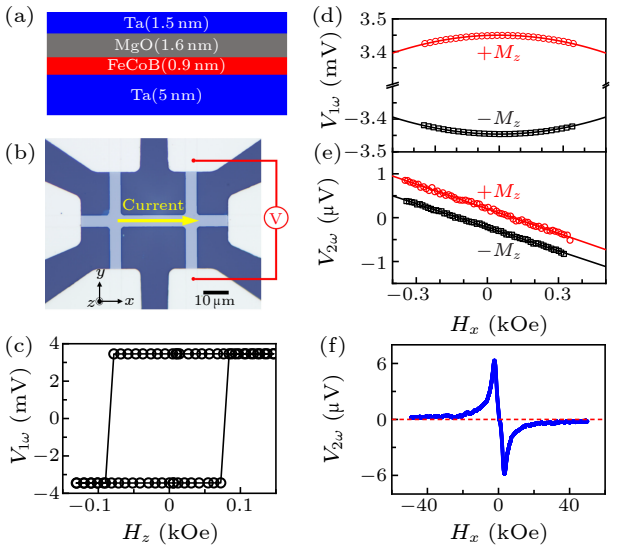

Fig. 2. Harmonic Hall voltage analysis of the Ta/FeCoB device. (a) Schematic of the magnetic stack. (b) Optical microscope image of the Hall bar device and the measurement coordinate. (c) First harmonic Hall voltage vs. perpendicular magnetic field. (d) First and (e), (f) second harmonic Hall voltages vs. the longitudinal magnetic field. $E = 62.7\,\mathrm{kV/m}$. The data in (e) are shifted for clarity.

synthetic antiferromagnets (SAFs),[15–19] collinear antiferromagnets (e.g., Fe_2O_3),[22] non-collinear antiferromagnets (e.g., Mn_3Sn),[20] van der Waals ferromagnets (Fe_3GeTe_2),[24] spin valve trilayers,[25] etc. Considerable claims have also been made from such switching angle shift analyses, including anisotropic self-induced SOTs in single-layer (Ga,Mn)(As,P)[27] and dramatic enhancement of the SOT efficiencies of transverse spins by magnetization compensation in SAFs[15] (which is inconsistent with the fundamental physics that the competing spin relaxation mechanism of spin–orbit scattering that scatters spins into the lattice should diminish the SOTs at full compensation[7]). However, it was barely verified whether domain wall depinning—the basis for switching angle shift analysis—was indeed the dominant switching mechanism for practical magnetic heterostructures.

Recently, experiments[27,33–38] have revealed that domain wall depinning, both quantitatively and qualitatively, fails to describe the switching current density of perpendicular magnetization in practical samples. The domain wall depinning analysis of the critical switching current density is found to yield tens of times misestimation of the SOT efficiency.[33,34] The domain wall depinning cannot explain the strongly asymmetric magnetization switching driven by a magnetic field or by an in-plane current.[35–38] These advances suggest an urgent need to reevaluate the accuracy and impact of the switching angle shift technique and unveil the in-depth switching mechanisms.

Here, we demonstrate that the switching angle shift analysis breaks down both qualitatively and quantitatively for magnetic heterostructures commonly used in spintronics. Experiments indicate that $\Delta\beta$ of magnetic bilayers typically includes a significant current-irrelevant contribution and a linear-in-current contribution that yields several times misestimation of ξ^j_{DL} if the switching angle shift analysis is applied.

For this work, we first sputter-deposited a prototype magnetic stack of Ta(5)/FeCoB(0.9)/MgO(1.6)/Ta(1.5) [Fig. 2(a), where the numbers are layer thicknesses in nm, FeCoB = $Fe_{60}Co_{20}B_{20}$] and several control samples (see below) on thermally oxidized silicon substrates at room temperature. The saturation magnetization of the FeCoB layer is ≈1260 emu/cm^3 as measured using a superconducting quantum interference device. The samples are patterned into 5 μm × 60 μm Hall bar devices [Fig. 2(b)] by photolithography and argon ion milling for transport measurements. The Ta/FeCoB devices are annealed at 210 ℃ for 20 min to enhance PMA. The resistivity (ρ_{xx}) of the Ta layer is 220 μΩ·cm as calibrated from the conductance enhancement of the Ta(5)/FeCoB(0.9)/MgO(1.6)/Ta(1.5) relative to the control stack Ta(1)/FeCoB(0.9)/MgO(1.6)/Ta(1.5).

We characterize the magnetic anisotropy and the SOTs of the samples using the well-recognized harmonic Hall voltage measurement in the low-field macrospin regime.[5,8,39] The in-phase first and out-of-phase second harmonic Hall voltages, $V_{1\omega}$ and $V_{2\omega}$, are collected using a lock-in amplifier as a function of the magnetic fields while a sinusoidal electric field of $E = 62.7\,\mathrm{kV/m}$ is applied onto the 60 μm-long Hall bar. As revealed by the first harmonic Hall voltage hysteresis driven by the perpendicular magnetic field (H_z) in Fig. 2(c), the Ta/FeCoB device exhibits good PMA, sharp magnetization switching, large perpendicular coercivity (H_c) of ≈80 Oe, and high anomalous Hall voltage (V_{AH}) of 3.45 mV. As shown in Figs. 2(d) and 2(e), the $V_{1\omega}$ and $V_{2\omega}$ data of the device are parabolic and linear functions of the longitudinal magnetic field (H_x), respectively, indicating that the device behaves as a rigid macrospin when tilted slightly from its easy axis by an in-plane field H_x of ≤0.3 kOe (the same

is true for data measured as a function of transverse field H_y). This allows accurate determination of PMA field (H_k) and H_{DL} from low-field harmonic Hall voltage analysis based on macrospin model,[8] i.e.,

$$V_{1\omega} = V_{AH}(1 - H_x^2/2H_k^2), \tag{3}$$

$$H_{DL} = -2\frac{\partial V_{2\omega}}{\partial H_x}\Big/\frac{\partial^2 V_{1\omega}}{\partial^2 H_x} - 2H_k V_{ANE,z}/V_{AHE}, \tag{4}$$

where $V_{ANE,z}$ is the anomalous Nernst voltage that we measure from the $V_{2\omega}$ value at very high positive H_x in Fig. 2(f). H_k is 2880 Oe as estimated from the fit of the data to Eq. (3) in Fig. 2(d). With $H_{DL} = 8.8 \pm 0.2$ Oe estimated using Eq. (4) and $j = E/\rho_{xx}$, the efficiency of the dampinglike SOT is then estimated as $\xi^j_{DL} = -0.105 \pm 0.001$ for the Ta/FeCoB device following the macrospin relation

$$\xi^j_{DL} = (2e/\hbar)\mu_0 M_s t_{FM} H_{DL}/j. \tag{5}$$

Next, we perform the switching angle shift measurement on the same Ta/FeCoB device. As shown in Fig. 3(a), we sweep the elevation angle (β) of the magnetic field (H_{xz}) with a fixed magnitude of 2.5 kOe (greater than H_k) near the positive ($+x$ direction, $\beta \to 0°$) and negative ($-x$ direction, $\beta \to 180°$) current directions and determine the shift $\Delta\beta$ of the switching angle loop under different bias direct currents (I). In Fig. 3(b), we summarize $\Delta\beta$ of the Ta/FeCoB device as a function of total direct current for $H_{xz} = 2.5$ kOe. As expected by the switching angle shift model [Fig. 1(c)], $\Delta\beta$ does show good linear scaling with I, with a slope of $\partial(\Delta\beta)/\partial I = -0.19°/\text{mA}$. However, with this slope from linear scaling, the domain wall depinning model [Eq. (2)] only yields a ξ^j_{DL} of -0.037 for Ta/FeCoB, which is about three times smaller than its true value (-0.105 as estimated from harmonic Hall voltage analysis). This deviation is consistent with our previous reports that domain wall depinning analysis of the switching current in thin-film and van der Waals magnets may misestimate torque efficiency by up to tens of times.[33,34] More strikingly, the linear fit of $\Delta\beta$ vs. I data also yields a nonzero intercept [Fig. 3(b)], indicating a nonzero perpendicular effective magnetic field at zero direct current. This observation cannot be explained by the domain wall depinning model.[3,28–32]

In Fig. 3(c), we further plot the $\Delta\beta$ values measured for different H_{xz} and the separated in-plane field-antisymmetric (β_0) and in-plane field-symmetric components ($\Delta\beta - \beta_0$). β_0 is irrelevant to the sign and

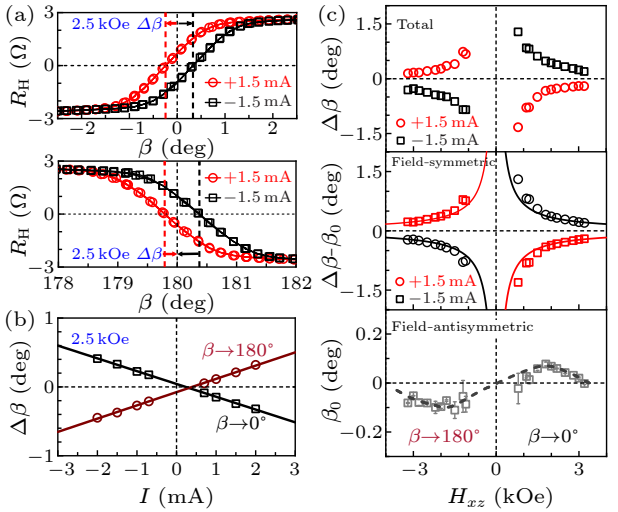

Fig. 3. Switching angle shift analysis. (a) Hall resistance vs. the magnetic field angle measured at a total current of $I = \pm 1.5$ mA and a magnetic field of $H_{xz} = 2.5$ kOe. (b) Switching angle shift ($\Delta\beta$) vs. current measured at β around 0° or 180° and a magnetic field of 2.5 kOe; the solid lines represent the best linear fits. (c) Dependences on H_{xz} of $\Delta\beta$, $\Delta\beta - \beta_0$, and β_0. The solid black and red curves plot the best inverse field fits of the data, while the dashed dark gray curve is to guide the eyes.

magnitude of the direct current in the Hall-bar device and thus cannot be attributed to any SOTs of spins or any thermal effects. $\Delta\beta - \beta_0$ switches sign upon reversal of the current direction and scales inversely with H_{xz} only at high fields but not at lower fields. Both the presence of the field-antisymmetric β_0 and the low-field deviation of field-symmetric $\Delta\beta - \beta_0$ from inverse field scaling [Fig. 3(c)] disagree with the switching angle shift model.

We emphasize that the breakdown of the switching angle shift technique is universal rather than just specific to the Ta/FeCoB devices. We have experimentally verified that the switching angle shift technique misestimates the SOTs typically by more than 2 times for a variety of other magnetic devices with different spin Hall metals and magnetic layers (e.g., Pt/Co, $Pt_{75}Ti_{25}/[Co/Ni]_3$, and $Au_{25}Pt_{75}$/Co in Table 1). The breakdown of the switching angle shift technique cannot be attributed to the presence of any perpendicularly polarized spin currents[40] or perpendicular Oersted field,[41] the generation of which requires a nonzero direct current and electric asymmetries within the device. The coherent rotation model is also unlikely to explain the switching of these Hall-bar devices [e.g., the gradual switching in Fig. 4(a)].

Table 1. Comparison of the SOT efficiencies (ξ^j_{DL}) estimated from the harmonic Hall voltage and switching angle shift analyses.

Samples	H_k (kOe)	ξ^j_{DL}		
		Harmonic Hall voltage	Switching angle shift ($H_{xz} = 2.5$ kOe)	Ratio
Ta 5/FeCoB 0.9	2.9	-0.105 ± 0.001	-0.037	3
Pt 4/Co 1	10.6 ± 0.1	0.219 ± 0.003	0.029 ± 0.003	7
$Au_{25}Pt_{75}$ 4/Co 0.64	6.6 ± 0.1	0.305 ± 0.013	0.153	2
$Pt_{75}Ti_{25}$ 2/[Co 0.25/Ni 0.25]$_3$	4.1	0.18	0.064	2.8

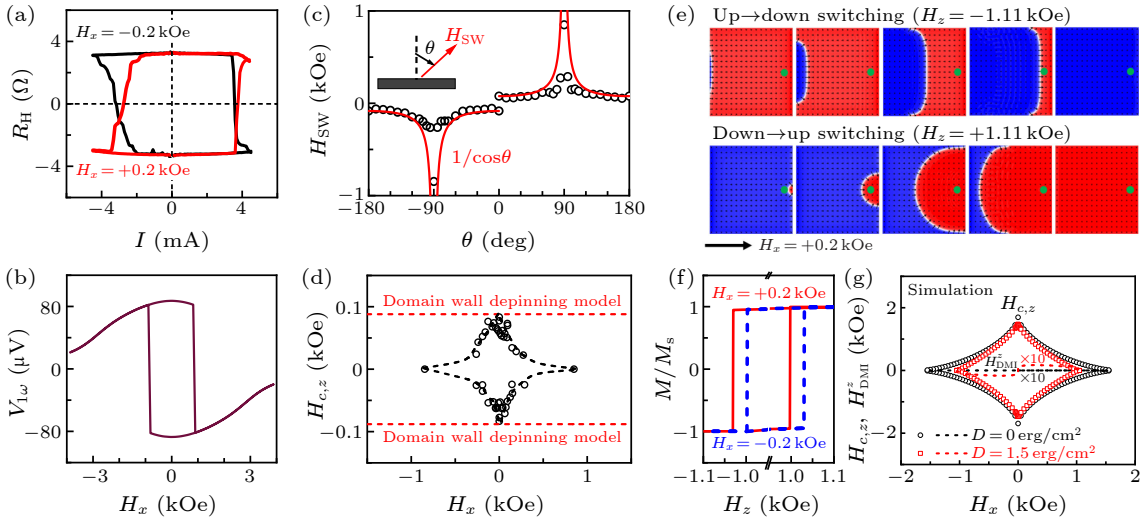

Fig. 4. Deviation from the domain wall depinning switching model. (a) Hall resistance vs. the total in-plane current under a longitudinal magnetic field of $H_x = \pm 200$ Oe, revealing a sizable shift induced by the in-plane magnetic field. (b) First harmonic Hall voltage vs. H_x, revealing sharp switching of the perpendicular magnetization by the in-plane magnetic field. (c) Dependence of the total switching field on its polar angle (θ); the red curve plots of the $1/\cos\theta$ fit, indicating strong deviation of the data from domain wall depinning at around $\pm 90°$. (d) Perpendicular coercivity ($H_{c,z}$) vs. H_x. The red dashed lines indicate the predicted $H_{c,z}$ values from the domain-wall depinning switching model. Small electric field of $E = 1.57$ kV/m for measurement of (b)–(d) to assure minimal influence of Joule heating. Micromagnetic simulation results: (e) z field-driven up-down and down-up switching process ($H_x = +0.2$ kOe, $D = 1.5$ erg/cm^2; the green dot near the right edge marks the location of a weak PMA region), (f) hysteresis loops ($H_x = \pm 0.2$ kOe, $D = 1.5$ erg/cm^2), and (g) dependences on H_x of $H_{c,z}$ (circles and squares) and intralayer DMI field H^z_{DMI} (dashed lines, multiplied by 10 for clarity) for a PMA device with $D = 0$ (black) and 1.5 erg/cm^2 (red).

We show below that the breakdown of the switching angle shift analysis arises because its base assumption, i.e., the domain depinning model, fails to capture the major characteristics of magnetization switching. The domain depinning assumption includes four characteristics,[3,32,35,41–44] i.e., (i) the same current magnitudes for the SOT switching of perpendicular magnetization under a given in-plane magnetic field H_x, (ii) no switching of perpendicular magnetization by any in-plane magnetic fields, (iii) a $1/\cos\theta$ scaling of the switching magnetic field (i.e., $H_{sw} = H_{c,z}/\cos\theta$) at different polar angles (θ), and (iv) a constant perpendicular coercivity ($H_{c,z}$) under different in-plane fields. Experimentally, the current switching hysteresis is shifted to the left side under a negative H_x but to the right side under a positive H_x [Fig. 4(a)]. The Ta/FeCoB device exhibits sharp switching driven solely by H_x in Fig. 4(b). As shown in Fig. 4(c), the switching field collected by sweeping the amplitude of the H_{xz} field at fixed polar angles (θ) also remarkably deviates near $\theta \approx \pm 90°$ (in-plane directions) from $1/\cos\theta$ scaling. In addition, the perpendicular coercivity $H_{c,z}$ also decreases with increasing H_x towards zero [Fig. 4(d)]. Thus, none of the characteristics of domain wall depinning switching is fulfilled in the studied samples.

These switching characteristics of the practical samples are highly suggestive of a coercivity reduction and a chiral perpendicular effective magnetic field induced by the in-plane magnetic field, which we reproduce below using micromagnetic simulations with field-driven nucleation but without domain wall depinning (zero pinning field). Following the long-range intralayer Dzyaloshinskii–Moriya interaction (DMI) model that a chiral perpendicular magnetic field can arise from the collective chiral coupling of magnetic domains with anisotropy fluctuations,[35] we simulate in Figs. 4(e)–4(g) the switching process of a 500 nm × 500 nm × 1 nm PMA device (with a unit cell size of 1 nm × 1 nm × 1 nm) that hosts a weaker-PMA 30 nm-in-diameter circular region near the center of the right edge [marked by a green dot in Fig. 4(e)] as a function of the in-plane magnetic field. Other parameters include the exchange stiffness $A = 0.8$ μerg/cm,[45,46] $M_s = 1260$ emu/cm^3, the DMI constant $D = 0$ and 1.5 erg/cm^2, and $H_k = 2.75$ kOe for the weak PMA region and 2.80 kOe for the rest region (this is a rather weak anisotropy variation, less than 1.8%).

As shown in Fig. 4(e), in the presence of both DMI and anisotropy fluctuations, the down-up switching (driven by a positive H_z) and up-down switching (driven by a negative H_z) undergo asymmetric nucleation (different nucleation fields) and propagation processes due to the H_x-triggered DMI coupling of the strong and weak PMA regions. Here, we stress that while critical for the asymmetry of the switching, the tiny anisotropy fluctuations, as is usually the case for high-quality samples, are too weak to affect the location of anti-domain nucleation such that anti-domains always nucleate at the center of left or right edges due to interfacial DMI.[47] Macroscopic consequences are that the in-plane magnetic field induces a rapid decrease of $H_{c,z}$ towards zero in the presence/absence of DMI [Fig. 4(g)] and a small hysteresis shift [Fig. 4(f)] that varies anti-symmetrically and non-monotonically with H_x only in the presence of a perpendicular intralayer

DMI field [$H^z_{\rm DMI}$, represented by the red dashed curve in Fig. 4(g)]. Such chiral asymmetric nucleation effect reasonably explains the seemingly puzzling experimental results in Figs. 3(c) and 4(a)–4(d). Switching of the PMA device by an in-plane field can be expected when $H_{c,z}$ becomes zero or less than intralayer DMI field. These results suggest a critical role for chiral asymmetric nucleation in switching perpendicular magnetization. It is also important to note that, in absence of DMI effects (i.e., at zero DMI and/or zero anisotropy fluctuations), nucleation fields also decrease rapidly with an in-plane magnetic field but symmetrically [Fig. 4(g)].

In conclusion, we have demonstrated from experiments and micromagnetic simulations that the popular "switching angle shift" technique can yield considerable misestimates for the SOTs of magnetic heterostructures. We find that the inaccuracy of the "switching angle shift" analysis arises because its base assumption, the simplifying domain wall depinning model, has not captured the remarkable, widespread in-plane magnetic field effects that arise most likely from chiral anisotropic nucleation. These findings suggest that switching angle shift analysis is not a universal technique for SOT characterization but should be limited to samples strictly fulfilling the conventional domain wall depinning model; the latter can be experimentally verified by its four characteristics specified above. We note that it is unrealistic to expect a universal analytical description of the relation between switching angle shift and SOTs, e.g., via a simple modification of Eq. (1), for various magnetic samples (e.g., magnetic single layers, heavy metal/magnet bilayers, or SAF trilayers) with switching dominated by or involved with chiral asymmetric nucleation due to considerable complications arising from the interplay of magnetization switching, various DMI effects (i.e., bulk, intralayer, interlayer DMIs),[35,47–52] and anisotropy fluctuations.[35] Moreover, this work also provides chiral asymmetric nucleation as a potential microscopic mechanism for understanding various magnetization switching puzzles such as in-plane field induced coercivity variation [Fig. 4(d)], non-linear current dependence of shifting fields,[53–55] large discrepancies in spin-torque efficiencies from switching angle/field shift analysis and others,[56] intralayer DMI fields,[35] asymmetric switching [Fig. 4(f)], and misestimation of SOT efficiency from domain wall depinning analysis of switching current.[33] This work will stimulate further efforts towards more precise and in-depth understanding of magnetization switching (the central topic of spintronics) and rechecking considerable literature claims relying on switching angle shift and domain wall depinning analysis.

Acknowledgements. This work was supported by the National Key Research and Development Program of China (Grant No. 2022YFA1204000), and partly by the National Natural Science Foundation of China (Grant Nos. 12274405, 12304155, and 12393831), and the Beijing Natural Science Foundation (Grant No. Z230006).

References

[1] Liu L Q, Pai C F, Li Y, Tseng H W, Ralph D C, and Buhrman R A 2012 *Science* **336** 555
[2] Miron I M, Garello K, Gaudin G, Zermatten P J, Costache M V, Auffret S, Bandiera S, Rodmacq B, Schuhl A and Gambardella P 2011 *Nature* **476** 189
[3] Zhu L J 2023 *Adv. Mater.* **35** 2300853
[4] Luo Z C, Hrabec A, Dao T P, Sala G, Finizio S, Feng J, Mayr S, Raabe J, Gambardella P, and Heyderman L J 2020 *Nature* **579** 214
[5] Zhu L J, Ralph D C, and Buhrman R A 2018 *Phys. Rev. Appl.* **10** 031001
[6] Zhu L J, Zhu L J, Shi S J, Sui M L, Ralph D C, and Buhrman R A 2019 *Phys. Rev. Appl.* **11** 061004
[7] Zhu L J and Ralph D C 2023 *Nat. Commun.* **14** 1778
[8] Zhu L J, Li J W, Zhu L J, and Xie X Y 2022 *Phys. Rev. Appl.* **18** 064052
[9] Han J H, Richardella A, Siddiqui S A, Finley J, Samarth N, and Liu L Q 2017 *Phys. Rev. Lett.* **119** 077702
[10] Dc M, Grassi R, Chen J Y, Jamali M, Reifsnyder Hickey D R, Zhang D L, Zhao Z Y, Li H S, Quarterman P, Lv Y, Li M, Manchon A, Mkhoyan K A, Low T, and Wang J P 2018 *Nat. Mater.* **17** 800
[11] Zhu L J, Zhu L J, and Buhrman R A 2021 *Phys. Rev. Lett.* **126** 107204
[12] Wu H, Zhang P, Deng P, Lan Q Q, Pan Q J, Razavi S A, Che X Y, Huang L, Dai B Q, Wong K, Han X F, and Wang K L 2019 *Phys. Rev. Lett.* **123** 207205
[13] Yan Z H, Li Z X, Zhu L J, Lin X, and Zhu L J 2025 *Chin. Phys. Lett.* **42** 090701
[14] Zhang C L, Fukami S, DuttaGupta S, Sato H, and Ohno H 2018 *Jpn. J. Appl. Phys.* **57** 04FN02
[15] Zhang P X, Liao L Y, Shi G Y, Zhang R Q, Wu H Q, Wang Y Y, Pan F, and Song C 2018 *Phys. Rev. B* **97** 214403
[16] Saito Y, Ikeda S, Inoue H, and Endoh T 2023 *IEEE Trans. Magn.* **59** 1
[17] Fan H D, Jin M H, Wu B R, Wei M Z, Wang J L, Shao Z J, Yu C Q, Wen J H, Li H, Li W J, and Zhou T J 2023 *Appl. Phys. Lett.* **122** 262404
[18] Fan H D, Jin M H, Luo Y M, Yang H X, Wu B R, Feng Z S, Zhuang Y S, Shao Z L, Yu C Q, Li H, Wen J H, Wang N N, Liu B, Li W J, and Zhou T J 2023 *Adv. Funct. Mater.* **33** 2211953
[19] Saito Y, Ikeda S, and Endoh T 2022 *Phys. Rev. B* **105** 054421
[20] Yoon J Y, Zhang P X, Chou C T, Takeuchi Y, Uchimura T, Hou J T, Han J H, Kanai S, Ohno H, Fukami S, and Liu L Q 2023 *Nat. Mater.* **22** 1106
[21] Liu L Q, Lee O J, Gudmundsen T J, Ralph D C, and Buhrman R A 2012 *Phys. Rev. Lett.* **109** 096602
[22] Zhang P X, Chou C T, Yun H H, McGoldrick B C, Hou J T, Mkhoyan K A, and Liu L Q 2022 *Phys. Rev. Lett.* **129** 017203
[23] Jiang M, Asahara H, Sato S, Kanaki T, Yamasaki H, Ohya S, and Tanaka M 2019 *Nat. Commun.* **10** 2590
[24] Zhang Y, Xu H J, Yi C J, Wang X, Huang Y, Tang J, Jiang J L, He C L, Zhao M K, Ma T Y, Dong J, Guo C Y, Feng J F, Wan C H, Wei H X, Du H F, Shi Y G, Yu G Q, Zhang G Y, and Han X F 2021 *Appl. Phys. Lett.* **118** 262406
[25] Zhang R Q, Su J, Cai J W, Shi G Y, Li F, Liao L Y, Pan F, and Song C 2019 *Appl. Phys. Lett.* **114** 092404
[26] Park S, Lee K J, Han K, Lee S, Liu X Y, Dobrowolska M, and Furdyna J K 2022 *Appl. Phys. Lett.* **121** 112403
[27] Park S, Lee K J, Lee S, Liu X Y, Dobrowolska M, and Furdyna J K 2021 *APL Mater.* **9** 101102
[28] Thiaville A, Rohart S, Jué É, Cros V, and Fert A 2012 *EPL* **100** 57002

[29] Bhowmik D, Nowakowski M E, You L, Lee O, Keating D, Wong M, Bokor J, and Salahuddin S 2015 *Sci. Rep.* **5** 11823

[30] Baumgartner M, Garello K, Mendil J, Avci C O, Grimaldi E, Murer C, Feng J, Gabureac M, Stamm C, Acremann Y, Finizio S, Wintz S, Raabe J, and Gambardella P 2017 *Nat. Nanotechnol.* **12** 980

[31] Pai C F, Mann M, Tan A J, and Beach G S 2016 *Phys. Rev. B* **93** 144409

[32] Lee O J, Liu L Q, Pai C F, Li Y, Tseng H W, Gowtham P G, Park J P, Ralph D C, and Buhrman R A 2014 *Phys. Rev. B* **89** 024418

[33] Zhu L J, Ralph D C, and Buhrman R A 2021 *Phys. Rev. Appl.* **15** 024059

[34] Lin X and Zhu L J 2023 *Mater. Today Electron.* **4** 100037

[35] Liu Q B, Liu L, Xing G Z, and Zhu L J 2024 *Nat. Commun.* **15** 2978

[36] Yu G Q, Upadhyaya P, Wong K L, Jiang W J, Alzate J G, Tang J, Amiri P K, and Wang K L 2014 *Phys. Rev. B* **89** 104421

[37] Fan W J, Zhao J, Tang M, Chen H J, Yang H, Lü W M, Shi Z, and Qiu X P 2019 *Phys. Rev. Appl.* **11** 034018

[38] Hao Q and Xiao G 2015 *Phys. Rev. B* **91** 224413

[39] Hayashi M, Kim J, Yamanouchi M, and Ohno H 2014 *Phys. Rev. B* **89** 144425

[40] Liu Q B, Lin X, Shaked A, Nie Z Y, Yu G Q, and Zhu L J 2024 *Adv. Mater.* **36** 2406552

[41] Liu Q B and Zhu L J 2022 *Appl. Phys. Rev.* **9** 041401

[42] Kondorsky E 1940 *J. Phys. USSR* **2** 161

[43] Schumacher F 1991 *J. Appl. Phys.* **70** 3184

[44] Zhu L J, Zhu L J, Liu Q B, and Lin X 2023 *Phys. Rev. B* **108** 014420

[45] Kim J S, Kim G, Jung J, Jung K, Cho J, Kim W Y, and You C Y 2022 *Sci. Rep.* **12** 4549

[46] Yamanouchi M, Jander A, Dhagat P, Ikeda S, Matsukura F, and Ohno H 2011 *IEEE Magn. Lett.* **2** 3000304

[47] Pizzini S, Vogel J, Rohart S, Buda-Prejbeanu L D, Jué E, Boulle O, Miron I M, Safeer C K, Auffret S, Gaudin G, and Thiaville A 2014 *Phys. Rev. Lett.* **113** 047203

[48] Fernandez-Pacheco A, Vedmedenko E, Ummelen F, Mansell R, Petit D, and Cowburn R P 2019 *Nat. Mater.* **18** 679

[49] Han D S, Lee K, Hanke J P, Mokrousov Y, Kim K W, Yoo W, van Hees Y L W, Kim T W, Lavrijsen R, You C Y, Swagten H J M, Jung M H, and Kläui M 2019 *Nat. Mater.* **18** 703

[50] Avci C O, Lambert C, Sala G, and Gambardella P 2021 *Phys. Rev. Lett.* **127** 167202

[51] Zhu L J, Zhu L J, Ma X, Li X Q, and Buhrman R A 2022 *Commun. Phys.* **5** 151

[52] Zhu L J, Lujan D, and Li X Q 2024 *Sci. China-Phys. Mech. Astron.* **67** 227511

[53] Dohi T, Fukami S, and Ohno H 2021 *Phys. Rev. B* **103** 214450

[54] Wu Y Z, Wu T, Chen H R, Cui Y W, Xu H Y, Jiang N, Cheng Z, and Wu Y Z 2025 *Appl. Phys. Lett.* **126** 012401

[55] Yang Q, Han D, Zhao S S, Kang J M, Wang F, Lee S C, Lei J Y, Lee K J, Park B G, and Yang H 2024 *Nat. Commun.* **15** 1814

[56] Zhu L J, Ralph D C, and Buhrman R A 2021 *Appl. Phys. Rev.* **8** 031308